



Article

Amyloid-Forming Corpora Amylacea and Spheroid-Type Amyloid Deposition: Comprehensive Analysis Using Immunohistochemistry, Proteomics, and a Literature Review

Shojiro Ichimata ^{1,*}, Yukiko Hata ¹, Tsuneaki Yoshinaga ², Nagaaki Katoh ², Fuyuki Kametani ³, Masahide Yazaki ⁴, Yoshiki Sekijima ² and Naoki Nishida ¹

¹ Department of Legal Medicine, Faculty of Medicine, University of Toyama, Toyama 930-0194, Japan

² Department of Medicine (Neurology and Rheumatology), Shinshu University School of Medicine, Matsumoto 390-8621, Japan; kiccho828@gmail.com (T.Y.)

³ Department of Brain and Neurosciences, Tokyo Metropolitan Institute of Medical Science, Tokyo 156-8506, Japan; kametani-fy@igakuken.or.jp

⁴ Institute for Biomedical Sciences, Shinshu University, Matsumoto 390-8621, Japan; mayazaki@shinshu-u.ac.jp

* Correspondence: ichimata@med.u-toyama.ac.jp

Abstract: This study aimed to elucidate the similarities and differences between amyloid-forming corpora amylacea (CA) in the prostate and lung, examine the nature of CAs in cystic tumors of the atrioventricular node (CTAVN), and clarify the distinctions between amyloid-forming CA and spheroid-type amyloid deposition. We conducted proteomics analyses using liquid chromatography–tandem mass spectrometry with laser microdissection and immunohistochemistry to validate the characteristics of CAs in the lung and prostate. Our findings revealed that the CAs in these organs primarily consisted of common proteins (β 2-microglobulin and lysozyme) and locally produced proteins. Moreover, we observed a discrepancy between the histopathological and proteomic analysis results in CTAVN-associated CAs. In addition, while the histopathological appearance of the amyloid-forming CAs and spheroid-type amyloid deposits were nearly identical, the latter deposition lacked β 2-microglobulin and lysozyme and exhibited evident destruction of the surrounding tissue. A literature review further supported these findings. These results suggest that amyloid-forming CAs in the lung and prostate are formed through a shared mechanism, serving as waste containers (wastesomes) and/or storage for excess proteins (functional amyloids). In contrast, we hypothesize that while amyloid-forming CA and spheroid-type amyloid deposits are formed, in part, through common mechanisms, the latter are pathological.

Keywords: amyloid; beta-2 micro-globulin; corpora amylacea; functional amyloids; lactoferrin; lysosome; macrophage; pulmonary surfactant protein



Citation: Ichimata, S.; Hata, Y.; Yoshinaga, T.; Katoh, N.; Kametani, F.; Yazaki, M.; Sekijima, Y.; Nishida, N. Amyloid-Forming Corpora Amylacea and Spheroid-Type Amyloid Deposition: Comprehensive Analysis Using Immunohistochemistry, Proteomics, and a Literature Review. *Int. J. Mol. Sci.* **2024**, *25*, 4040. <https://doi.org/10.3390/ijms25074040>

Academic Editor: Carlos Gutierrez-Merino

Received: 6 March 2024

Revised: 31 March 2024

Accepted: 3 April 2024

Published: 4 April 2024



Copyright: © 2024 by the authors. Licensee MDPI, Basel, Switzerland. This article is an open access article distributed under the terms and conditions of the Creative Commons Attribution (CC BY) license (<https://creativecommons.org/licenses/by/4.0/>).

1. Introduction

Corpora amylacea (CA) has been described in various human organs, including the brain, lungs, and prostate [1–4]. CA primarily involves two different types of lesions: one is a polyglucosan structure similar to starch, which is positive by periodic acid–Schiff staining, whereas the other is an aggregate of certain types of fibrillary proteins that stain positively for Congo red (CR) and thioflavin [1]. Although these are histopathologically distinct lesions, they are believed to share a common function as wastesomes [1]. Amyloid-forming CA formation is frequently observed in the prostate and lungs [1,5,6]. Several histopathological and biochemical studies have evaluated the CA of the prostate [7,8], but few studies have examined CA in the lung. Furthermore, there have been no studies examining the similarities and differences between CAs at the two sites.

Cystic tumor of the atrioventricular node (CTAVN) is a rare, benign lesion located at the base of the atrial septum, around the area of the AVN in the human heart. CAs are a

histopathological feature of CTAVN [4,9]. These deposits may have amyloid properties because of their green birefringence under polarized light [9]; however, there has been no characterization of these deposits, particularly as to whether they contain amyloid-associated proteins, based on proteomic analyses.

Spheroid-type amyloid deposition (STAD) is a rare form of amyloidosis [10–12]. This pattern of deposition often appears as a localized form, but it can also be associated with systemic amyloidosis. Morphologically, amyloid-forming CA and STAD are very similar; however, the latter lesions often occur in association with tumors or cause damage to surrounding tissues, which suggests that they are pathologically distinct lesions. To our knowledge, no studies have thoroughly examined the differences between these lesions.

The objectives of this study were as follows: (1) elucidate the similarities and differences between amyloid-forming CAs in the prostate and lung; (2) determine the nature of CAs in CTAVN; and (3) clarify the differences between amyloid-forming CA and STAD. We conducted proteomics analyses using liquid chromatography–tandem mass spectrometry (LC-MS/MS) with laser microdissection (LMD) in a patient with pulmonary and prostatic amyloid-forming CAs. Immunohistochemistry was performed in a series of three patients with pulmonary CA and three patients with prostatic CA to validate the results of the proteomic analyses. Moreover, we performed the same proteomic analysis in a patient with CTAVN-associated CR-positive CA. To address the third objective, we re-evaluated the results of our previously reported histopathologic and proteomic analyses of a STAD patient [10]. Finally, we reviewed prior histopathological studies on STAD and compared their findings with those obtained in the present study on amyloid-forming CA.

2. Results

2.1. General Appearance of Pulmonary, Prostatic, and CTAVN-Associated CAs

We selected three cases of pulmonary CA, three cases of prostatic CA, three cases of CA associated with CTAVN, and one case of STAD from the archives of all medicolegal autopsy patients from our department between January 2008 and August 2023. A summary of the cases is presented in Table 1.

Table 1. Demographic data associated with cases of corpora amylacea (CA).

Case #	Pulmonary CA Cases			Prostatic CA Cases			CTAVN Cases		
	Case 1 *	Case 2	Case 3	Case 1 *	Case 2	Case 3	Case 1	Case 2	Case 3
Age	75	90	85	75	88	45	36	45	76
Sex	M	F	F	M	M	M	F	M	M
Cause of death	HyT	MN	Drowning	HyT	ACD	KA	SCD	SCD	SCD
Dialysis	None	None	None	None	None	None	None	None	None

Abbreviations: ACD, acute cardiac dysfunction; CTAVN, cystic tumor of the atrioventricular node; F, female; HyT, hypothermia; KA, ketoacidosis; M, male; MN, malnutrition; SCD, sudden cardiac death. * Same patient.

2.2. General Appearance of Pulmonary, Prostatic, and CTAVN-Associated CAs

Representative histopathological microphotographs are shown in Figure 1.

Generally, all the CAs exhibited round, eosinophilic deposits with concentric laminations by H&E staining (Figure 1a–c). The pulmonary CAs exhibited a relatively uniform size and shape, with weak-to-moderate congophilia, and they exhibited clear apple-green birefringence under polarized light observation (Figure 1a,d,g). In contrast, the prostatic CAs varied in size and shape, with strong congophilia and distinct apple-green birefringence under polarized light (Figure 1b,e,h). The CTAVN-associated CAs also varied in size and shape, with weak-to-moderate congophilia, and with only some displaying apple-green birefringence under polarized light (Figure 1c,f,i). In addition, macrophages were observed around the CAs in the lung (Figure 1a) and prostate (Figure 1b) but not around the CTAVN-associated CAs (Figure 1c). There was no evident destruction of the surrounding tissue by the CAs in all cases.

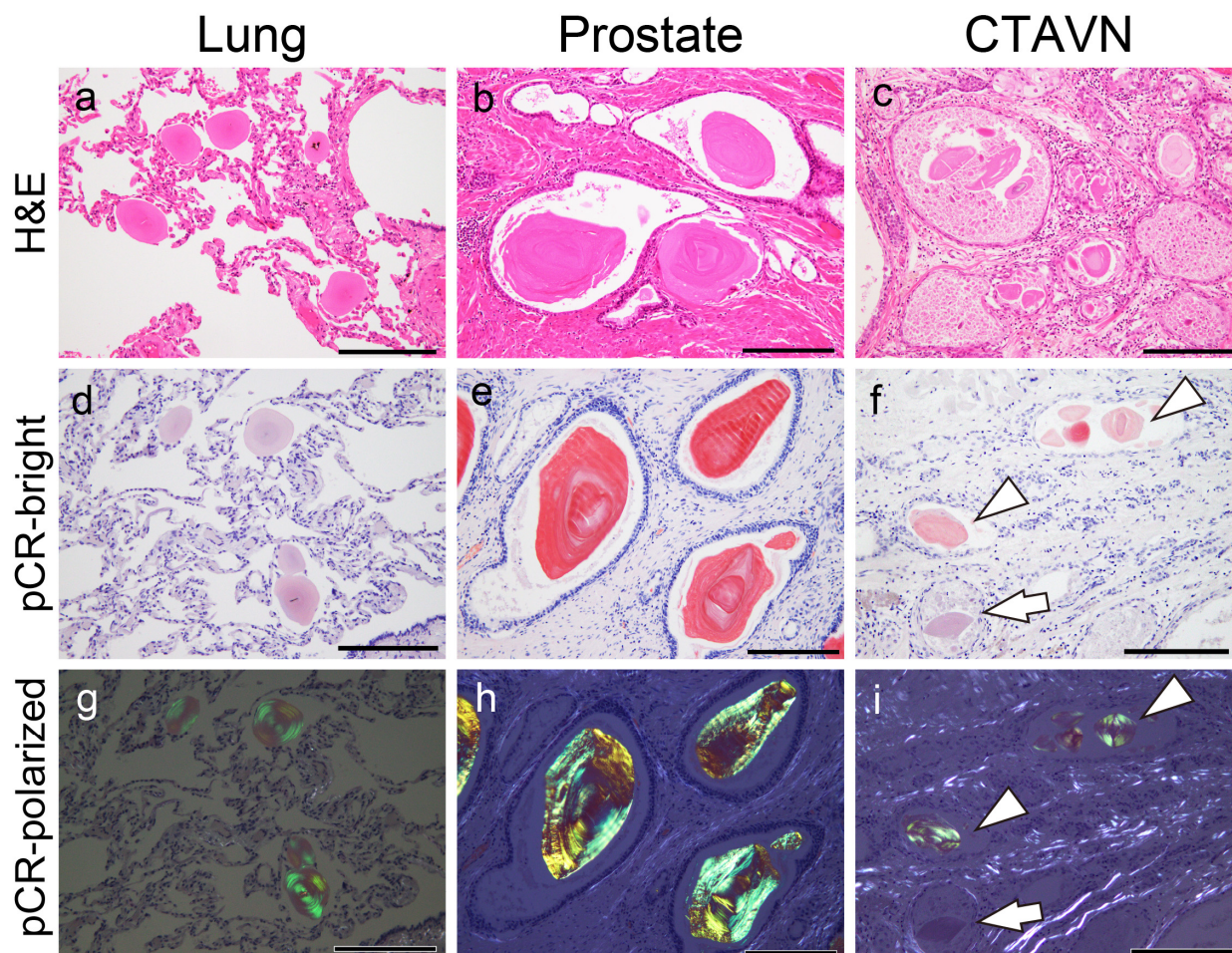


Figure 1. Representative microphotographs of pulmonary and prostatic CAs and CTAVN-associated CAs in the heart. (a,d,g) Pulmonary CA Case 1; (b,e,h) prostatic CA Case 1; (c,f,i) CTAVN Case 1. (a–c) Hematoxylin and eosin (H&E) staining; (d–f) phenol Congo red (pCR) staining with a bright field; (g–i) pCR staining under polarized light. (a–c) All CAs were round with eosinophilic deposits showing concentric laminations upon H&E staining. Note that macrophages were observed around CAs in the lung (a), and multinucleated giant cells were observed around CAs in the prostate (b). (d,e,g,h) Almost all pulmonary and prostatic CAs exhibited congophilia with apple-green birefringence under polarized light. Although CTAVN-associated CAs showed congophilic deposits (f), some CAs (arrow) lacked apple-green birefringence under polarized light (arrowheads indicate CAs showing typical apple-green birefringence). Scale bar = 200 μ m (a–i).

2.3. Proteomic and Immunohistochemical Features of Pulmonary CAs

A summary of the proteomics results and representative microphotographs of the pulmonary CAs in Case 1 are shown in Figure 2. Additional microphotographs of the pulmonary CAs in all three cases are provided in Supplementary Figure S1.

LC-MS/MS with LMD detected five proteins thought to be amyloidogenic, as shown in Figure 2a. Immunohistochemical localization within the CAs was confirmed for β 2-microglobulin (Figure 2b), lysozyme C (Figure 2c), pulmonary surfactant protein (PSP)-A, and PSP-B (Figure 2d,e). Immunohistochemistry for lactoferrin yielded negative results (Figure 2f), whereas focal p62 immunoreactivity was observed (Figure 2g).

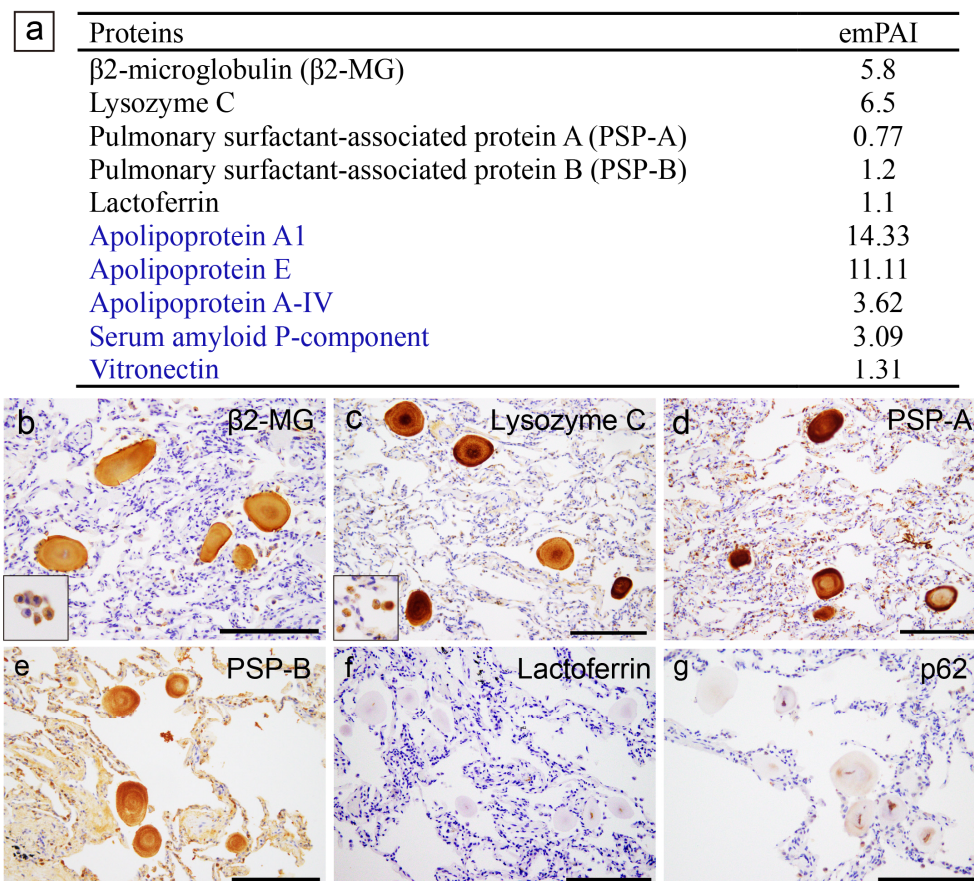


Figure 2. Representative proteomics results and immunohistochemistry micrographs based on these results in the lung. (a) Proteins identified in the CAs using laser microdissection and liquid chromatography–tandem mass spectrometry (LMD and LC-MS/MS) in pulmonary CA Case 1; immunohistochemistry for β 2-microglobulin (β 2-MG) (b); lysozyme C (c); pulmonary surfactant protein A (PSP-A) (d); PSP-B (e); lactoferrin (f); and p62 (g). (a) In addition to some amyloid-associated proteins (shown in blue), five amyloidogenic proteins were detected [13]. Of these, immunoreactivity for β 2-MG (b), lysozyme C (c), PSP-A (d), and PSP-B (e) was confirmed, whereas no immunoreactivity for lactoferrin was observed (f). The macrophages were also positive for β 2-MG and lysozyme C (insets in panels b,c). Weak p62 immunoreactivity was observed in the central area of some CAs. The emPAI is the exponentially modified protein abundance index, which is used as an index for estimating relative protein quantification in mass-spectrometry-based proteomic analyses. Scale bar = 200 μ m (b–g).

2.4. Proteomic and Immunohistochemical Features of Prostatic CAs

A summary of the proteomics results for the prostatic CAs in Case 1, along with representative microphotographs of Cases 1 and 2, are shown in Figure 3. Representative microphotographs of the prostatic CAs for all three cases are provided in Supplementary Figure S2.

In addition to some amyloid-associated proteins, three proteins that may be amyloidogenic were detected by LC-MS/MS with LMD (Figure 3a), which is consistent with previous studies [7,8]. Immunohistochemistry revealed that all the CAs were positive for lysozyme C (Figure 3b) and lactoferrin (Figure 3c). Focally, p62 immunoreactivity was identified (Figure 3d). Interestingly, eosinophilic deposits showing moderate congophilia and apple-green birefringence under polarized light were identified within a few carcinoma glands (Figure 3e–g); however, lysozyme C, lactoferrin, and p62 were not detected in these deposits by immunohistochemistry (Figure 3h–j).

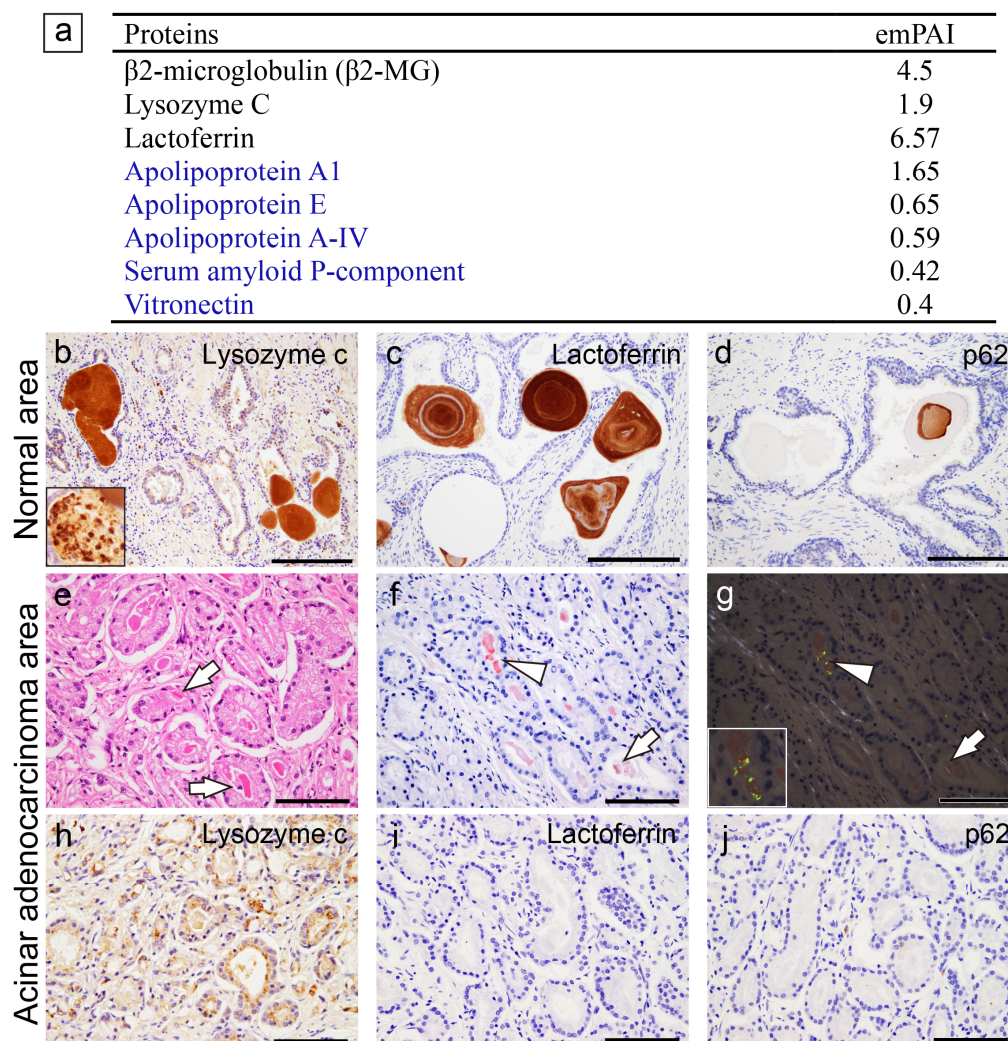


Figure 3. Representative proteomics results and immunohistochemistry micrographs based on the results in the prostate. (b–d) CAs observed within the normal gland area; (e–j) eosinophilic deposits observed within the acinar adenocarcinoma glands. (a) Proteins identified in the CA lesions using LMD and LC-MS/MS in prostatic CA Case 1; immunohistochemistry for lysosome C (b,h); lactoferrin (c,i); p62 (d,j); H&E staining (e); pCR staining under a bright field (f) and a polarized field (g). (a) In addition to some amyloid-associated proteins (shown in blue), three amyloidogenic proteins were detected. VA lesions were positive for lysozyme C (b) and lactoferrin (c). The macrophages were also positive for lysozyme C (inset in panel b). p62 immunoreactivity in the central area of some CAs (d). Within the tumor glands, eosinophilic deposits, including crystalloids (arrow), were evident (e). (f,g) Some of the deposits showed weak-to-moderate congophilia and exhibited apple-green birefringence under polarized light (arrowhead, inset is a higher magnification view of the deposit). Crystalloids were weakly positive for pCR but did not exhibit apple-green birefringence under polarized light (arrow). In addition, these eosinophilic deposits were not immunoreactive for lysozyme C (h), lactoferrin (i), or p62 (j). Scale bar = 200 μ m (b–d); 100 μ m (e–j).

2.5. Comparison of the Amino Acid Sequences of Proteins Commonly Identified in Pulmonary and Prostatic CAs

The amino acid sequences and identified peptide sequences of β 2-microglobulin, lysozyme C, and lactoferrin in the lungs and prostate are shown in Figure 4.

For β 2-microglobulin and lysozyme C, nearly identical regions were identified in the lung and prostate (Figure 4a–d); however, for lactoferrin, only a small portion was identified in the lung (Figure 4e), particularly on the C-terminal end, whereas almost the

entire length of lactoferrin was identified in the prostate (Figure 4f). The detected PSP-A and PSP-B peptide sequences are shown in Supplementary Figure S3.

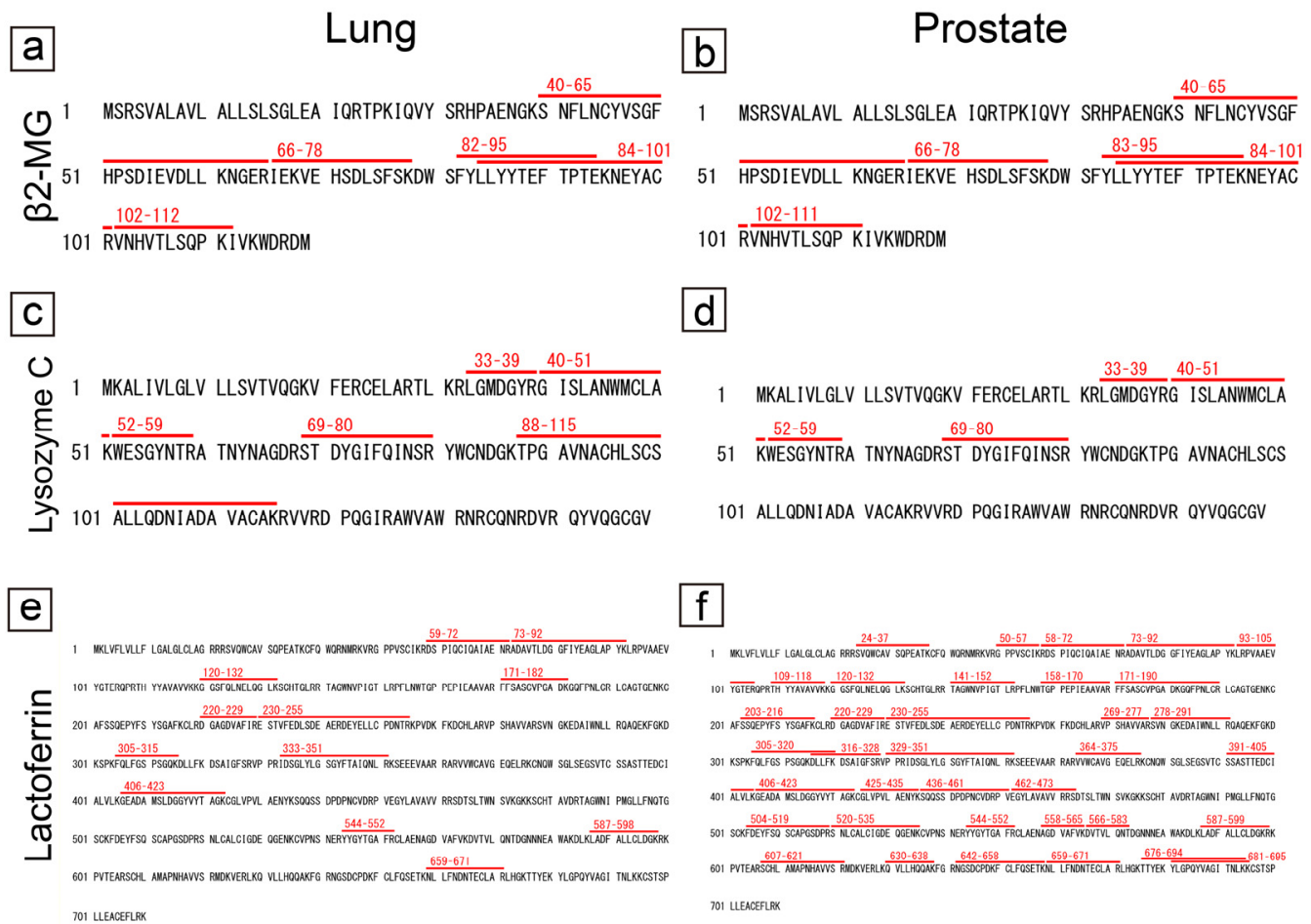


Figure 4. Proteomics results for the amyloidogenic proteins commonly observed in pulmonary and prostatic CAs. (a,c,e) Lung; (b,d,f) prostate; (a,b) β2-MG; (c,d) lysozyme C; and (e,f) lactoferrin. Detected peptides, which had a peptide score of 30 or higher by MASCOT analysis, are shown in red. (a–d) Regarding β2-MG and lysozyme C, similar peptides were detected in the lung and prostate. (e,f) In contrast, for lactoferrin, only a few peptide sequences were identified in the lungs, whereas several sequences were identified in the prostate.

2.6. Proteomic and Immunohistochemical Features of CTAVN-Associated CAs

A summary of the proteomics results and representative microphotographs of the immunohistochemistry in Case 1 are shown in Figure 5.

In contrast to the pulmonary and prostatic CAs, we did not detect amyloid-associated or reported amyloidogenic proteins in the CTAVN-associated CAs by LC-MS/MS with LMD (Case 1); however, consistent with our previous report [4], olfactomedin 4 was detected in the CAs (Figure 5a,b). The CAs of all three cases exhibited weak-to-strong immunoreactivity for olfactomedin 4 (Figure 5c–e). In contrast, p62 immunoreactivity was identified only in Case 1 (Figure 5f–h). The representative findings for all three CTAVN cases are shown in Supplementary Figure S4.

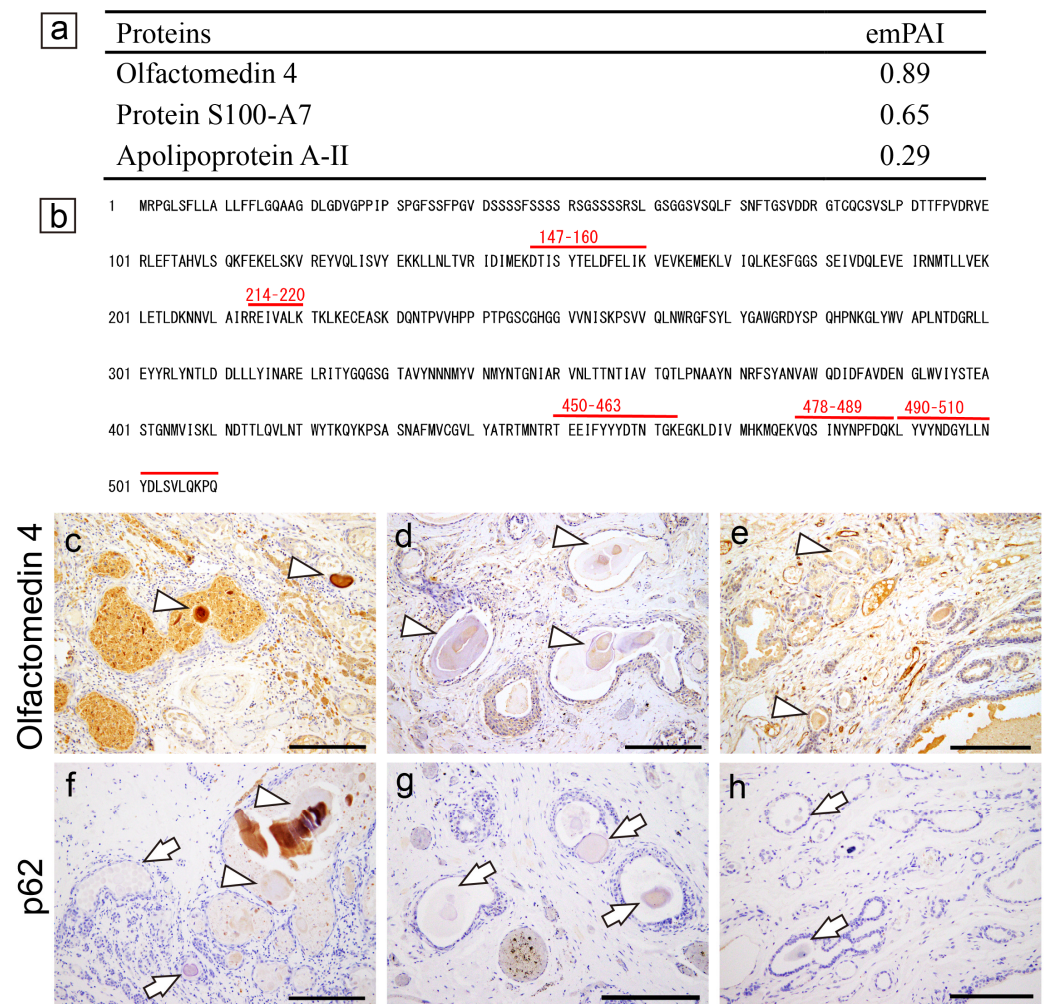


Figure 5. Representative proteomics results and immunohistochemistry micrographs of the heart. (a–c,f) CTAVN Case 1; (d,g) CTAVN Case 2; (e,h) CTAVN Case 3. (a) Proteins identified in the CAs using LMD and LC-MS/MS in CTAVN Case 1; (b) detected peptide sequences of olfactomedin 4; immunohistochemistry for olfactomedin 4 (c–e); p62 (f–h). (a,b) Consistent with our previous immunohistochemistry-based study [4], olfactomedin 4 was identified in CAs and CA-like deposits within CTAVN glands. No amyloid-associated proteins were identified. Detected peptides, which had a peptide score of 30 or higher by MASCOT analysis, are shown in red (b). Immunohistochemistry for olfactomedin 4 was strongly positive in Case 1 (c) and weakly positive in Case 2 (d) and Case 3 (e) (arrowheads indicate olfactomedin-4-positive deposits). In contrast, immunohistochemistry for p62 was from negative to partially positive in Case 1 (f), whereas it was negative in Cases 2 (g) and 3 (h) (arrowheads indicate olfactomedin-4-positive deposits and arrows indicate negative deposits). Scale bar = 200 μ m (c–h).

2.7. Proteomic and Immunohistochemical Features of STAD Associated with Systemic Amyloid Immunoglobulin Light Chain (AL) Amyloidosis

Representative microphotographs are shown in Figure 6.

In this case, the shape of the amyloid deposits was similar to that of the CAs, particularly in the prostate; however, the destruction of surrounding tissue by the deposits was evident. Furthermore, although some amyloid-associated proteins and seven peptides from the immunoglobulin light chain lambda variable region were detected, β 2-microglobulin and lysozyme C were not detected. Furthermore, there was no p62 immunoreactivity in the deposits.

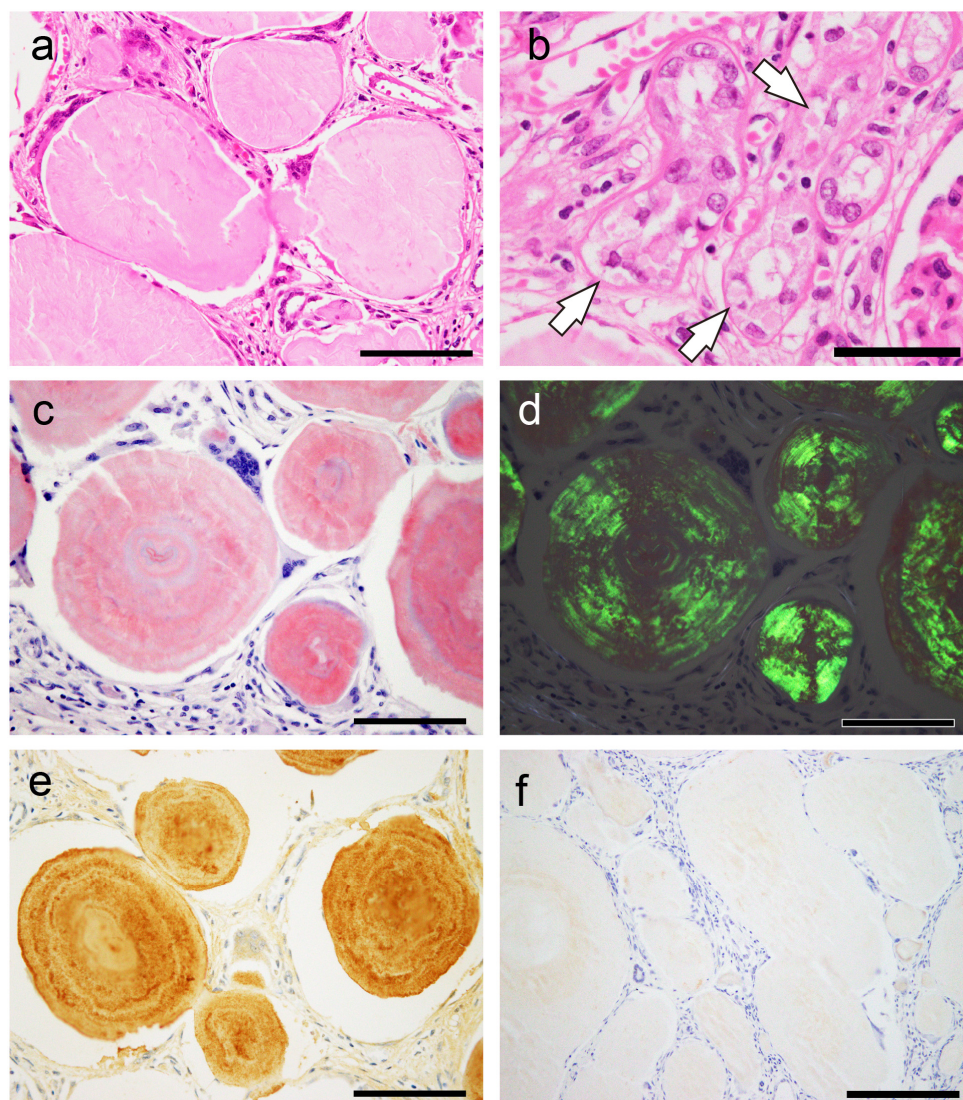


Figure 6. Representative microphotographs of spheroid-type amyloid deposition in the kidney. (a,b) H&E staining; pCR staining under a bright field (c) and polarized light (d); immunohistochemistry for Ig λ (e); p62 (f). (a,b) Spheroid-type amyloid deposits were evident in the interstitium (a) and in the tubules (b, arrow). (c,d) These deposits were positive for pCR (c) and exhibited apple-green birefringence under polarized light (d). (e) As shown in our previous report, the deposits were positive by immunohistochemistry for Ig λ . (f) In contrast, immunohistochemistry for p62 was negative. Scale bar = 200 μ m (f); 100 μ m (a–e).

2.8. Literature Review of Previous Reports on STAD

To further characterize STAD, we conducted a comprehensive literature review and have summarized the results in Table 2 [10–12,14–45].

STAD was observed in both localized and systemic amyloidosis. Although the size and morphology varied between cases and among the organs, the deposits appeared to show concentric laminations in most cases. In addition, the presence of histiocytes and multinucleated giant cells was noted around the deposits in some cases, suggesting that they may be involved in the formation of the deposits [10,11]. These features are similar to those observed in amyloid-forming CAs. Consistent with our results, immunohistochemistry and proteomics analysis did not identify β 2-microglobulin or lysozyme C in the deposits, and tissue damage resulting from the deposits was believed to have occurred in almost all STAD cases.

Table 2. Summary of previous reports of spheroid-type amyloid deposition (STAD).

Location	S/L	Concomitant Findings	Immunohistochemical Analysis	Proteomic Analysis
Stomach and small intestine [14]	S	Bronchiectasis, FMF, and renal failure	Pos: AA; Neg: β 2MG, TTR, Ig κ , Ig λ , CD68	NE
Small intestine [15,16]	L	Polypoid lesions	Pos: Ig λ ; Neg: AA, β 2MG, TTR, Ig κ [15] Pos: AP, AA, Ig κ , Ig λ (uneven) [16]	NE
Vater ampulla [17]	L	NET	NE	NE
Colon, TI [12]	L	Adenocarcinoma	NE	AL λ
Colon [18–20]	L	Ulcerative lesions [18] and rounded lesions [19]	Pos: Ig λ [18]	NE
Liver [21–26]	S/L	Various diseases (See [21,22])	Pos: AP, AA; Neg: Ig κ , Ig λ [21] Pos: none; Neg: AP, AA, UB, TTR, Ig κ , Ig [23] Pos: AA; Neg: β 2MG, TTR, Ig κ , Ig λ [24] Pos: LECT2 or Ig; Neg: AA, β 2MG, TTR [26]	ALECT2 or AL [26]
Sino-nasal tract [27]	L	Nasal mass	Pos: Ig κ and Ig λ ($\kappa > \lambda$)	NE
Parotid gland [28]	L	Acinic cell carcinoma	NE	NE
URT [29]	S/L	Plasmacytoma	NE	NE
Bronchus [11]	L	Erythematous mass	Pos: Lac; Neg: AA, β 2MG, TTR, Ig κ , Ig λ	ALac
Bone [30–32]	L	Myeloma, malignant lymphoma (see [30])	Pos: Ig κ or Ig λ ; Neg: AA [30]	NE
Bone marrow [33]	S	PCP	Pos: Ig λ	NE
Ureter [34]	L	Hydronephrosis	NE (likely AA)	NE
Kidney [10]	S	PCP	Pos: Ig λ ; Neg: AA, β 2MG, TTR, Ig κ	AL λ
Uterine cervix [35–37]	L	Smooth mass [36], SCC [37,38]	Pos: AA; Neg: CK, Ig κ , Ig λ [35] Pos: CK; Neg: AA, TTR, Ig κ , Ig λ [36,37]	NE
Pituitary gland [38–44]	L	Prolactinoma	Pos: PRL; Neg: CK, vimentin, GFAP, GH, FSH, LH, TSH, ACTH, β -A4 [39,41,42]	NE
Breast [45] *	L	Mammary tumor	Pos: α -casein, Lac; Neg: AA, TTR, CK, Ig κ , Ig λ	NE

Abbreviations: AA, (serum) amyloid A; ACTH, adrenocorticotrophic hormone; AP, amyloid P component; CK, cytokeratin; FMF, familial Mediterranean fever; FSH, follicle-stimulating hormone; GFAP, glial fibrillary acidic protein; GH, growth hormone; Ig, immunoglobulin (light chain); L, localized; Lac, lactoferrin; LECT2, leukocyte chemotactic factor 2; LH, luteinizing hormone; NE, not evaluated; Neg, negative; NET, neuroendocrine tumor; PCP, plasma cell proliferation; Pos: positive; PRL, prolactin; S, systemic; SCC, squamous cell carcinoma; TI, terminal ileum; TSH, thyroid-stimulating hormone; UB, ubiquitin; URT, upper respiratory tract. * Found in two dogs.

3. Discussion

In the present study, we demonstrated that: (1) CAs in the lung and prostate are comprised of common proteins (β 2-microglobulin and lysozyme C) and locally produced proteins (PSP-A and PSP-B in the lung; lactoferrin in the prostate); (2) CAs associated with CTAVN exhibit typical histopathological features of amyloid, whereas LMD with LC-MS/MS did not detect amyloid-associated or amyloidogenic proteins; (3) STAD is morphologically similar to amyloid-forming CAs, but it differs because it causes tissue destruction and lacks β 2-microglobulin or lysozyme C deposition (4). p62 immunoreactivity was observed in amyloid-forming CAs but not in STAD.

Several proteomic and immunohistochemical analyses of prostatic CA have been reported [7,8,46–48]; however, to our knowledge, this is the first comprehensive analysis of pulmonary CA using both methods. CAs in the lung and prostate consist of common proteins (β 2-microglobulin and lysozyme C) and locally produced proteins. This suggests a common mechanism underlying the formation of CAs in the lungs and prostate. CAs are frequently identified in normal prostate tissue [49], and their presence does not appear to damage the surrounding tissues in the prostate and lung. Thus, we can speculate that CAs in these organs are formed for physiological reasons rather than serving a pathological function. Riba et al. proposed that CAs act as “wasteosomes” to sequester waste products [1,50]. In contrast, certain polypeptide hormones are stored in an amyloid-like β -sheet conformation in the pituitary gland, which are considered functional amyloids [13,51]. Thus, it has been hypothesized that certain proteins, especially those prone to form amyloid fibrils, are disposed of or stored as amyloid-forming CA. Partial p62 immunoreactivity supports the role of amyloid-forming CAs as wasteosomes. β 2-microglobulin and lysozyme C may be essential components for the formation of amyloid CAs.

Macrophages were observed around the CAs in both organs and were also positive for β 2-microglobulin and lysozyme C, suggesting that they play an important role in this mechanism. Dobashi et al. suggested that the concentrically laminated bodies in pulmonary CAs may be formed by sequential aggregation, fusion, coalescence, and compaction of degenerated alveolar macrophages [6]; however, it remains unclear whether they remove deposits, create them, or perform both functions. Further studies are needed to elucidate this mechanism, as it may contribute to the development of amyloid removal therapy.

There are four types of PSPs: hydrophilic PSP-A and PSP-D, and hydrophobic PSP-B and PSP-C [52]. In pulmonary CAs, proteomic analysis revealed PAP-A and PAP-B, whereas PSP-C, known to form amyloid fibrils [53], was not detected. These results were confirmed by immunohistochemistry and are consistent with those of a previous report [54]. To our knowledge, however, there are no reports of PAP-A and PSP-B forming amyloid fibrils. Thus, it is unclear whether the PSP-A and PSP-B proteins within the pulmonary CA form amyloid fibrils or are merely deposited. During the metabolism of PSPs, >50% is derived from recycling or catabolic events managed by functional cross-talk between alveolar type II cells and macrophages [52]. We hypothesize that excess or denatured PSPs are converted into CAs to be discarded or stored as a stable structure. It is noteworthy that if this serves a storage function, it may represent a form of functional amyloids [55].

We observed pCR-positive deposits not only in benign acini but also in cancer acini. Although CAs are primarily noted in benign acini, they have been identified in 0.4%–13% of cancer acini [49]. Therefore, the observation of amyloid-forming deposits in the lumen of cancer acini is not surprising; however, it is noteworthy that neither the tumor glands nor their luminal deposits were immunoreactive to lactoferrin. This is consistent with the proteomic results of Tekin et al. [47]. Thus, it is likely that the composition of amyloid deposits in cancer acini differs from those in benign acini, which may lead to the discovery of a novel amyloid precursor protein. However, it should be noted that given the presumed nonphysiological nature of secretions in cancer acini, there may be a discrepancy between the histological findings of the deposits and the results obtained from proteomic analysis, as illustrated in the case of CTAVN, which is discussed below. This is a topic for future consideration.

Interestingly, all CTAVN cases exhibited CAs positive for pCR staining and displayed apple-green birefringence under polarized light; however, proteomic analysis yielded divergent results, with no accumulation of amyloid-associated proteins. The precise reason for this discrepancy remains unknown. One hypothesis is that CTAVN CAs exhibit significant variation in the degree of amyloid fibril formation, given the substantial differences in the congophilia of each deposit. Consequently, it is plausible that only deposits lacking amyloid formation were selected during the LMD process. Another possibility is that congophilia is a false positive. Because CTAVN is a non-physiologic lesion, the CAs forming within the glands of CTAVN may have different properties compared with those in the lung or prostate. The immunohistochemical characteristics of the CTAVN epithelium are similar to those of the prostate epithelium [4]; however, the proteins comprising CA are distinctly different in the two tissues. Moreover, given the significant sex-dependent differences observed in the immunohistochemical properties of the epithelium of CTAVN [4], it is important to consider that the proteomic analysis of CAs from the female patients in this study may have generated results distinct from those of the prostate. It will be necessary to collect more cases of CTAVN and analyze whether amyloid fibrils are indeed formed in CAs associated with CTAVN.

Through morphological examination and a literature review, we demonstrated that amyloid-forming CAs and STADs exhibit morphological similarities; however, the former do not exhibit distinct destruction of the surrounding tissue, in contrast to STAD. Collectively, these findings suggest that the formation of characteristic deposition morphology in amyloid-forming CAs and STAD may be partially mediated by common mechanisms, whereas the former are more closely associated with physiological processes, while the latter is likely formed through pathological mechanisms. This is supported by the observa-

tion that p62 was partially positive in the amyloid-forming CAs, whereas it was negative in the STADs. Nevertheless, to our knowledge, there are limited studies showing the immunoreactivity of proteins related to waste substance processing and elimination, such as ubiquitin or p62, in STAD [3,23]. Additional research in this area is warranted.

In addition to a certain level of bias in our study population, this study was also limited by the small sample size, with only three cases with CA being evaluated for each organ. Additionally, potential sex differences were not evaluated given that prostate is a male-specific organ. Furthermore, only one case with STAD was evaluated. Finally, we did not explore structural variations in amyloid fibers in lung and prostate CAs or such differences between CAs and STADs, underscoring the need for further investigations employing cryogenic electron microscopy.

In conclusion, we present the findings of a comprehensive analysis that integrates proteomic analysis and immunohistochemistry for amyloid-forming CAs. A summary of the results is presented in Table 3.

Table 3. Summary of the properties of amyloid-forming CAs and STADs.

	Prostatic-CA	Pulmonary-CA	CTAVN-CA	STAD
Congophilia	Strong	Moderate–strong	Weak–moderate	Strong
Strength of the AGBR	Strong	Strong	Weak–moderate	Strong
Macrophages	Positive	Positive	Negative–positive	Positive
Presence of CPs	Positive	Positive	Negative	Negative
Presence of AAPs	Positive	Positive	Negative	Positive
p62-IR	Positive (focal)	Positive (focal)	Negative–positive (focal)	Negative

Abbreviations: AAPs, amyloid-associated proteins; AGBR, apple-green birefringence under polarized light; CPs, common proteins (β 2-microglobulin and lysozyme C); IR, immunoreactivity.

These results suggest that amyloid-forming CAs in the lung and prostate may be formed through a shared mechanism, serving as waste containers (wasteosomes) and/or storage for excess proteins (functional amyloids). It would be interesting if the human body intentionally employs structures that manifest distinctive amyloid fibril formation at the histological level. In contrast, in the CAs associated with CTAVN, there was a discrepancy between the histopathological and proteomic analysis results, highlighting the presence of nonphysiological functions of the epithelium in this disease. Furthermore, while amyloid-forming CA and STAD are formed, in part, by some common mechanisms, the former may have physiological origins, whereas the latter is pathological. If this shared mechanism exists, its elucidation will contribute to the development of amyloid removal therapy via approaches distinct from those using antibody-based methods. Moreover, the incidence of CAs increases with age [1,7], suggesting that age-related shifts in protein production and clearance may influence CA development. Given the association of many amyloidoses with aging, alterations in protein metabolism due to aging might be a critical factor in the underlying pathogenesis. Therefore, we speculate that by analyzing CA and identifying the specific protein metabolic mechanisms that are altered with aging, insights into approaches that can be utilized to prevent amyloid deposition may be gained.

4. Materials and Methods

4.1. Tissue Samples

Tissue specimens from the lung (for evaluating pulmonary CA), prostate (for evaluating prostatic CA), heart (for evaluating CTAVN-associated CA), and kidney (for evaluating STAD) were collected, fixed in 20% buffered formalin, and routinely embedded in paraffin. Then, 4 μ m thick sections were cut and stained with hematoxylin and eosin (H&E) or were analyzed by immunohistochemistry. Furthermore, 6 μ m thick sections were cut and stained with phenol CR (pCR) [56].

4.2. Histopathological Evaluation

The presence of CAs was determined using H&E-stained specimens. pCR-positive structures, which showed typical apple-green birefringence under polarized light, were histologically confirmed as amyloid deposits. Immunohistochemistry was performed to confirm the proteomics results. The immunohistochemistry methods used in this study are summarized in Supplementary Table S1. Immunostaining was performed using a Leica Bond-MAX automation system with Leica Refine detection kits (Leica Biosystems, Bannockburn, IL, USA) following the manufacturer's instructions. All sections were counterstained with hematoxylin.

4.3. Proteomics Analysis Using Mass Spectrometry

We used LMD followed by LC-MS/MS for analyzing CAs in the lung, prostate, and glands of CTAVN. The methods used for LMD with LC-MS/MS have been described previously [57,58].

Supplementary Materials: The supporting information can be downloaded from: <https://www.mdpi.com/article/10.3390/ijms25074040/s1>.

Author Contributions: Conceptualization, S.I.; data curation, S.I.; formal analysis, S.I.; funding acquisition, S.I.; investigation, S.I., Y.H., T.Y., N.K., F.K., M.Y. and Y.S.; methodology, F.K.; project administration, S.I.; resources, Y.H. and N.N.; supervision, N.N.; validation, N.N.; visualization, S.I.; writing—original draft, S.I.; writing—review and editing, Y.H., T.Y., N.K., F.K., M.Y., Y.S. and N.N. All authors have read and agreed to the published version of the manuscript.

Funding: This study was supported in part by a JSPS KAKENHI grant awarded to Shojiro Ichimata (grant number JP20K18979).

Institutional Review Board Statement: This study was approved by the Ethical Committee of Toyama University (I2020006) and followed the ethical standards established in the 1964 Declaration of Helsinki and updated in 2008.

Informed Consent Statement: Patient consent was waived due to the nature of forensic autopsy. However, to address ethical considerations as thoroughly as possible, we obtained approval from the University of Toyama Ethics Committee (I2020006) and posted an opt-out statement regarding the research on our department's website (http://www.med.u-toyama.ac.jp/legal/for_family.html).

Data Availability Statement: The datasets used and analyzed in the current study are available from the corresponding authors upon request.

Acknowledgments: The authors would like to thank Miyuki Maekawa for her technical assistance.

Conflicts of Interest: All authors declare no conflicts of interest.

Abbreviations

CA, corpora amylacea; CTAVN, cystic tumor of the atrioventricular node; pCR, phenol Congo red; H&E, hematoxylin and eosin; LC-MS/MS, liquid chromatography-tandem mass spectrometry; LMD, laser microdissection; PSP, pulmonary surfactant protein; STAD, spheroid-type amyloid deposition.

References

1. Riba, M.; Del Valle, J.; Auge, E.; Vilaplana, J.; Pelegri, C. From corpora amylacea to wasteosomes: History and perspectives. *Ageing Res. Rev.* **2021**, *72*, 101484. [[CrossRef](#)]
2. Hechtman, J.F.; Gordon, R.E.; McBride, R.B.; Harpaz, N. Corpora amylacea in gastrointestinal leiomyomas: A clinical, light microscopic, ultrastructural and immunohistochemical study with comparison to hyaline globules. *J. Clin. Pathol.* **2013**, *66*, 951–955. [[CrossRef](#)]
3. Hechtman, J.F.; Gordon, R.E.; Harpaz, N. Intramuscular corpora amylacea adjacent to ileal low-grade neuroendocrine tumours (typical carcinoids): A light microscopic, immunohistochemical and ultrastructural study. *J. Clin. Pathol.* **2013**, *66*, 566–572. [[CrossRef](#)]

4. Ichimata, S.; Hata, Y.; Yajima, N.; Katayama, Y.; Nomoto, K.; Nishida, N. Sex-dependent expression of prostatic markers and hormone receptors in cystic tumor of the atrioventricular node: A histopathological study of three cases. *Pathol. Int.* **2021**, *71*, 141–146. [[CrossRef](#)]
5. DuPre, N.C.; Flavin, R.; Sfanos, K.S.; Unger, R.H.; To, S.; Gazeeva, E.; Fiorentino, M.; De Marzo, A.M.; Rider, J.R.; Mucci, L.A.; et al. Corpora amylacea in prostatectomy tissue and associations with molecular, histological, and lifestyle factors. *Prostate* **2018**, *78*, 1172–1180. [[CrossRef](#)]
6. Dobashi, M.; Yuda, F.; Narabayashi, M.; Imai, Y.; Isoda, N.; Obata, K.; Umetsu, A.; Ohgushi, M. Histopathological study of corpora amylacea pulmonum. *Histol. Histopathol.* **1989**, *4*, 153–165.
7. Sfanos, K.S.; Wilson, B.A.; De Marzo, A.M.; Isaacs, W.B. Acute inflammatory proteins constitute the organic matrix of prostatic corpora amylacea and calculi in men with prostate cancer. *Proc. Natl. Acad. Sci. USA* **2009**, *106*, 3443–3448. [[CrossRef](#)]
8. Kanenawa, K.; Ueda, M.; Isoguchi, A.; Nomura, T.; Tsuda, Y.; Masuda, T.; Misumi, Y.; Yamashita, T.; Ando, Y. Histopathological and biochemical analyses of prostate corpora amylacea. *Amyloid* **2019**, *26*, 160–161. [[CrossRef](#)]
9. David, R.; Hiss, Y. Corpora amylacea in mesothelioma of the atrioventricular node. *J. Pathol.* **1978**, *124*, 111–116. [[CrossRef](#)]
10. Ichimata, S.; Hata, Y.; Abe, R.; Yoshinaga, T.; Katoh, N.; Kametani, F.; Yazaki, M.; Sekijima, Y.; Ehara, T.; Nishida, N. An autopsy case of amyloid tubulopathy exhibiting characteristic spheroid-type deposition. *Virchows Arch.* **2020**, *477*, 157–163. [[CrossRef](#)]
11. Ichimata, S.; Aoyagi, D.; Yoshinaga, T.; Katoh, N.; Kametani, F.; Yazaki, M.; Uehara, T.; Shiozawa, S. A case of spheroid-type localized lactoferrin amyloidosis in the bronchus. *Pathol. Int.* **2019**, *69*, 235–240. [[CrossRef](#)]
12. Kim, M.J.; McCroskey, Z.; Piao, Y.; Belcheva, A.; Truong, L.; Kurtin, P.J.; Ro, J.Y. Spheroid-type of AL amyloid deposition associated with colonic adenocarcinoma: A case report with literature review. *Pathol. Int.* **2018**, *68*, 123–127. [[CrossRef](#)]
13. Buxbaum, J.N.; Dispenzieri, A.; Eisenberg, D.S.; Fandrich, M.; Merlini, G.; Saraiva, M.J.M.; Sekijima, Y.; Westermarck, P. Amyloid nomenclature 2022: Update, novel proteins, and recommendations by the International Society of Amyloidosis (ISA) Nomenclature Committee. *Amyloid* **2022**, *29*, 213–219. [[CrossRef](#)]
14. Demirhan, B.; Bilezikci, B.; Kiyici, H.; Boyacioglu, S. Globular amyloid deposits in the wall of the gastrointestinal tract: Report of six cases. *Amyloid* **2002**, *9*, 42–46. [[CrossRef](#)]
15. Hemmer, P.R.; Topazian, M.D.; Gertz, M.A.; Abraham, S.C. Globular amyloid deposits isolated to the small bowel: A rare association with AL amyloidosis. *Am. J. Surg. Pathol.* **2007**, *31*, 141–145. [[CrossRef](#)]
16. Acebo, E.; Mayorga, M.; Fernando Val-Bernal, J. Primary amyloid tumor (amyloidoma) of the jejunum with spheroid type of amyloid. *Pathology* **1999**, *31*, 8–11. [[CrossRef](#)]
17. Malhotra, A.; Venugopal, S.; Ravindra, S. Unique spheroid deposits of amyloid in an ampullary neuroendocrine tumour. *Indian. J. Pathol. Microbiol.* **2022**, *65*, 226–228.
18. Diaz Del Arco, C.; Fernandez Acenero, M.J. Globular amyloidosis of the colon. *Arab. J. Gastroenterol.* **2018**, *19*, 96–99. [[CrossRef](#)]
19. Martín-Arranz, E.; Pascual-Turrión, J.M.; Martín-Arranz, M.D.; Burgos, E.; Froilán-Torres, C.; Adán-Merino, L.; Lorenzo, A.; Segura-Cabral, J.M. Focal globular amyloidosis of the colon. An exceptional diagnosis. *Rev. Esp. Enferm. Dig.* **2010**, *102*, 555–556. [[CrossRef](#)]
20. Harris, J.C.; Zhang, Q.; Tondon, R.; Alipour, Z.; Stashek, K. Characterization of amyloidosis in the gastrointestinal tract with an emphasis on histologically distinct interstitial patterns of deposition and misinterpretations. *Am. J. Surg. Pathol.* **2024**, *48*, 302–308. [[CrossRef](#)]
21. Makhlof, H.R.; Goodman, Z.D. Globular hepatic amyloid: An early stage in the pathway of amyloid formation: A study of 20 new cases. *Am. J. Surg. Pathol.* **2007**, *31*, 1615–1621. [[CrossRef](#)]
22. Agaram, N.; Shia, J.; Klimstra, D.S.; Lau, N.; Lin, O.; Erlandson, R.A.; Filippa, D.A.; Godwin, T.A. Globular hepatic amyloid: A diagnostic peculiarity that bears clinical significance. *Hum. Pathol.* **2005**, *36*, 845–849. [[CrossRef](#)]
23. Pilgaard, J.; Fenger, C.; Schaffalitzky de Muckadell, O.B. Globular amyloid deposits in the liver. *Histopathology* **1993**, *23*, 479–480. [[CrossRef](#)]
24. Osick, L.A.; Lee, T.P.; Pedemonte, M.B.; Jacob, L.; Chauhan, P.; Navarro, C.; Comer, G.M. Hepatic amyloidosis in intravenous drug abusers and AIDS patients. *J. Hepatol.* **1993**, *19*, 79–84. [[CrossRef](#)]
25. French, S.W.; Schloss, G.T.; Stillman, A.E. Unusual amyloid bodies in human liver. *Am. J. Clin. Pathol.* **1981**, *75*, 400–402. [[CrossRef](#)]
26. Chandan, V.S.; Shah, S.S.; Lam-Himlin, D.M.; Petris, G.D.; Mereuta, O.M.; Dogan, A.; Torbenson, M.S.; Wu, T.T. Globular hepatic amyloid is highly sensitive and specific for LECT2 amyloidosis. *Am. J. Surg. Pathol.* **2015**, *39*, 558–564. [[CrossRef](#)]
27. Kumar, B.; Pant, B.; Kumar, V.; Negi, M. Sinonasal globular amyloidosis simulating malignancy: A rare presentation. *Head. Neck Pathol.* **2016**, *10*, 379–383. [[CrossRef](#)]
28. Drut, R.; Giménez, P.O. Acinic cell carcinoma of salivary gland with massive deposits of globular amyloid. *Int. J. Surg. Pathol.* **2008**, *16*, 202–207. [[CrossRef](#)]
29. Michaels, L.; Hyams, V.J. Amyloid in localised deposits and plasmacytomas of the respiratory tract. *J. Pathol.* **1979**, *128*, 29–38. [[CrossRef](#)]
30. Pambuccian, S.E.; Horyd, I.D.; Cawte, T.; Huvos, A.G. Amyloidoma of bone, a plasma cell/plasmacytoid neoplasm. Report of three cases and review of the literature. *Am. J. Surg. Pathol.* **1997**, *21*, 179–186. [[CrossRef](#)]
31. Bauer, W.H.; Kuzma, J.F. Solitary tumors of atypical amyloid (paramyloid). *Am. J. Clin. Pathol.* **1949**, *19*, 1097–1112. [[CrossRef](#)] [[PubMed](#)]

32. Unal, F.; Hepgül, K.; Bayindir, C.; Bilge, T.; Imer, M.; Turantan, I. Skull base amyloidoma: Case report. *J. Neurosurg.* **1992**, *76*, 303–306. [[CrossRef](#)]
33. Bommannan, B.K.K.; Sonai, M.; Sachdeva, M.U. Bone marrow amyloid spherulites in a case of AL amyloidosis. *Blood Cells Mol. Dis.* **2016**, *58*, 19–20. [[CrossRef](#)]
34. Mantoo, S.; Hwang, J.S.; Chiang, G.S.; Tan, P.H. A rare case of localised AA-type amyloidosis of the ureter with spheroids of amyloid. *Singapore Med. J.* **2012**, *53*, e77–e79.
35. Gibbons, D.; Lindberg, G.M.; Ashfaq, R.; Saboorian, M.H. Localized amyloidosis of the uterine cervix. *Int. J. Gynecol. Pathol.* **1998**, *17*, 368–371. [[CrossRef](#)] [[PubMed](#)]
36. Gondo, T.; Ishihara, T.; Kawano, H.; Uchino, F.; Takahashi, M.; Iwata, T.; Matsumoto, N.; Yokota, T. Localized amyloidosis in squamous cell carcinoma of uterine cervix: Electron microscopic features of nodular and star-like amyloid deposits. *Virchows Arch. A Pathol. Anat. Histopathol.* **1993**, *422*, 225–231. [[CrossRef](#)]
37. Aho, H.J.; Talve, L.; Mäenpää, J. Acantholytic squamous cell carcinoma of the uterine cervix with amyloid deposition. *Int. J. Gynecol. Pathol.* **1992**, *11*, 150–155. [[CrossRef](#)]
38. Kitamura, K.; Nakayama, T.; Ohata, K.; Wakasa, K.; Miki, Y. Computed tomography and magnetic resonance imaging appearance of prolactinoma with spheroid-type amyloid deposition. *J. Comput. Assist. Tomogr.* **2011**, *35*, 313–315. [[CrossRef](#)] [[PubMed](#)]
39. Gul, S.; Bahadir, B.; Dusak, A.; Kalayci, M.; Edebali, N.; Acikgoz, B. Spherical amyloid deposition in a prolactin-producing pituitary adenoma. *Neuropathology* **2009**, *29*, 81–84. [[CrossRef](#)]
40. Kim, S.H.; Kim, S.H.; Lee, S.K.; Kim, T.S. Squash smear findings of spherical amyloid in pituitary prolactinoma. A case report. *Acta Cytol.* **2004**, *48*, 447–450. [[CrossRef](#)]
41. Hassan, T.; Ikeda, H.; Yoshimoto, T. Salmon roe-like amyloid deposition in a prolactinoma: A case report. *Brain Tumor Pathol.* **2003**, *20*, 89–92. [[CrossRef](#)] [[PubMed](#)]
42. Wiesli, P.; Brändle, M.; Brandner, S.; Kollias, S.S.; Bernays, R.L. Extensive spherical amyloid deposition presenting as a pituitary tumor. *J. Endocrinol. Investig.* **2003**, *26*, 552–555. [[CrossRef](#)]
43. Hinton, D.R.; Polk, R.K.; Linse, K.D.; Weiss, M.H.; Kovacs, K.; Garner, J.A. Characterization of spherical amyloid protein from a prolactin-producing pituitary adenoma. *Acta Neuropathol.* **1997**, *93*, 43–49. [[CrossRef](#)]
44. Kuratsu, J.; Matsukado, Y.; Miura, M. Prolactinoma of pituitary with associated amyloid-like substances. Case report. *J. Neurosurg.* **1983**, *59*, 1067–1070. [[CrossRef](#)] [[PubMed](#)]
45. Taniyama, H.; Kitamura, A.; Kagawa, Y.; Hirayama, K.; Yoshino, T.; Kamiya, S. Localized amyloidosis in canine mammary tumors. *Vet. Pathol.* **2000**, *37*, 104–107. [[CrossRef](#)] [[PubMed](#)]
46. Yanamandra, K.; Alexeyev, O.; Zamotin, V.; Srivastava, V.; Shchukarev, A.; Brorsson, A.C.; Tartaglia, G.G.; Vogl, T.; Kayed, R.; Wingsle, G.; et al. Amyloid formation by the pro-inflammatory S100A8/A9 proteins in the ageing prostate. *PLoS ONE* **2009**, *4*, e5562. [[CrossRef](#)]
47. Tekin, B.; Dasari, S.; Theis, J.D.; Vrana, J.A.; Murray, D.L.; Oglesbee, D.; Thompson, R.H.; Leibovich, B.C.; Boorjian, S.A.; Whaley, R.D.; et al. Mass spectrometry-based assessment of prostate cancer-associated crystalloids reveals enrichment for growth and differentiation factor 15. *Hum. Pathol.* **2023**, *135*, 35–44. [[CrossRef](#)]
48. Cross, P.A.; Bartley, C.J.; McClure, J. Amyloid in prostatic corpora amylacea. *J. Clin. Pathol.* **1992**, *45*, 894–897. [[CrossRef](#)] [[PubMed](#)]
49. Palangmonthip, W.; Wu, R.; Tarima, S.; Bobholz, S.A.; LaViolette, P.S.; Gallan, A.J.; Iczkowski, K.A. Corpora amylacea in benign prostatic acini are associated with concurrent, predominantly low-grade cancer. *Prostate* **2020**, *80*, 687–697. [[CrossRef](#)]
50. Riba, M.; Campo-Sabariz, J.; Tena, I.; Molina-Porcel, L.; Ximelis, T.; Calvo, M.; Ferrer, R.; Martin-Venegas, R.; Del Valle, J.; Vilaplana, J.; et al. Wasteosomes (corpora amylacea) of human brain can be phagocytosed and digested by macrophages. *Cell Biosci.* **2022**, *12*, 177. [[CrossRef](#)]
51. Maji, S.K.; Perrin, M.H.; Sawaya, M.R.; Jessberger, S.; Vadodaria, K.; Rissman, R.A.; Singru, P.S.; Nilsson, K.P.; Simon, R.; Schubert, D.; et al. Functional amyloids as natural storage of peptide hormones in pituitary secretory granules. *Science* **2009**, *325*, 328–332. [[CrossRef](#)]
52. Pioselli, B.; Salomone, F.; Mazzola, G.; Amidani, D.; Sgarbi, E.; Amadei, F.; Murgia, X.; Catinella, S.; Villetti, G.; De Luca, D.; et al. Pulmonary surfactant: A unique biomaterial with life-saving therapeutic applications. *Curr. Med. Chem.* **2022**, *29*, 526–590. [[CrossRef](#)]
53. Gustafsson, M.; Thyberg, J.; Naslund, J.; Eliasson, E.; Johansson, J. Amyloid fibril formation by pulmonary surfactant protein C. *FEBS Lett.* **1999**, *464*, 138–142. [[CrossRef](#)]
54. Yamanouchi, H.; Yoshinouchi, T.; Watanabe, R.; Fujita, J.; Takahara, J.; Ohtsuki, Y. Immunohistochemical study of a patient with diffuse pulmonary corpora amylacea detected by open lung biopsy. *Intern. Med.* **1999**, *38*, 900–903. [[CrossRef](#)]
55. Otzen, D.; Riek, R. Functional amyloids. *Cold Spring Harb. Perspect. Biol.* **2019**, *11*, a033860. [[CrossRef](#)]
56. Ishii, W.; Matsuda, M.; Nakamura, N.; Katsumata, S.; Toriumi, H.; Suzuki, A.; Ikeda, S. Phenol Congo red staining enhances the diagnostic value of abdominal fat aspiration biopsy in reactive AA amyloidosis secondary to rheumatoid arthritis. *Intern. Med.* **2003**, *42*, 400–405. [[CrossRef](#)]

57. Kametani, F.; Haga, S. Accumulation of carboxy-terminal fragments of APP increases phosphodiesterase 8B. *Neurobiol. Aging* **2015**, *36*, 634–637. [[CrossRef](#)] [[PubMed](#)]
58. Abe, R.; Katoh, N.; Takahashi, Y.; Takasone, K.; Yoshinaga, T.; Yazaki, M.; Kametani, F.; Sekijima, Y. Distribution of amyloidosis subtypes based on tissue biopsy site—Consecutive analysis of 729 patients at a single amyloidosis center in Japan. *Pathol. Int.* **2021**, *71*, 70–79. [[CrossRef](#)] [[PubMed](#)]

Disclaimer/Publisher’s Note: The statements, opinions and data contained in all publications are solely those of the individual author(s) and contributor(s) and not of MDPI and/or the editor(s). MDPI and/or the editor(s) disclaim responsibility for any injury to people or property resulting from any ideas, methods, instructions or products referred to in the content.